

---

# Characterization of turbulent natural and mixed convection in confined enclosures equipped with a heat source

Sihem Bouzid<sup>1</sup>, Yamina Harnane<sup>1,\*</sup>, Abdelhafidh Brima<sup>2</sup>

1. Department of Mechanical Engineering, Faculty of Sciences and Applied Sciences, University of Larbi ben M'hidi Oum El Bouaghi, 04000, Algeria

2. Mechanical Engineering Laboratory (LGM), University of Mohamed Khider Biskra, 07000, Algeria

*harnaney@gmail.com*

---

**ABSTRACT.** In this numerical study two configurations are considered, the first configuration in natural convection corresponds to a closed cavity equipped with a heating bar and the second mixed configuration corresponds to the same cavity but ventilated. The flow is turbulent ( $Gr_H = 1,2.10^8$ ), a choice of model is very important. The turbulence model chosen for natural convection is the low-Reynolds  $k-\epsilon$  model. A comparison of the turbulence models led us to choose the RNG  $k-\epsilon$  model for mixed convection study, because it is the suitable model for flows in ventilated cavities as well as flows with recirculation. Ventilation effect on natural flow has been studied by analyzing flow dynamic and thermal structure. Nusselt average number on each bar face is found to be improved by jet injection into the ventilated cavity, from about 50% to 60%. This comparison reveals the different velocities influence of the incoming air jet on the confined cavity flow structure, or this jet succeeds in breaking the single-cell flow of natural convection case into a multicellular flow for the other case of mixed convection at high velocities above the heating bar, of which it is the main purpose of this study.

**RÉSUMÉ.** Dans cette étude numérique deux configurations sont considérées, la première configuration en convection naturelle correspond à une cavité fermée munie d'un barreau chauffant et la deuxième configuration mixte correspond à la même cavité mais ventilée. L'écoulement est turbulent ( $Gr_H = 1,2.10^8$ ), un choix du modèle est très important. Le modèle de turbulence choisi pour la convection naturelle est le modèle  $k-\epsilon$  bas-Reynolds. Une comparaison des modèles de turbulence nous a mené à choisir le modèle  $k-\epsilon$  RNG pour l'étude de la convection mixte, parce que c'est le modèle approprié aux écoulements dans les cavités ventilées ainsi qu'aux écoulements avec recirculation. L'effet de la ventilation sur l'écoulement naturelle a été étudié en analysant la structure dynamique et thermique de l'écoulement. Le nombre de Nusselt moyen sur chaque face du barreau est trouvée améliorée par l'injection du jet dans la cavité ventilée, d'environ 50% à 60%. Cette comparaison nous révèle l'influence des différentes vitesses du jet d'air entrant sur la structure de l'écoulement de la cavité confinée, ou ce jet réussit à briser l'écoulement monocellulaire du cas de la convection

*naturelle en un écoulement multicellulaire pour l'autre cas de convection mixte à des vitesses élevée au-dessus du barreau chauffant, dont il est le but principal de cette étude.*

*KEYWORDS: Fluent, turbulence model, CFD, heat transfer, Closed cavities, ventilated cavities.*

*MOTS-CLÉS: fluent, modèle de turbulence k-ε, LRN (k-ε bas Reynolds), CFD, Transfert de chaleur, cavités fermées, cavités ventilées, nusselt.*

DOI:10.3166/I2M.17.63-79 © 2018 Lavoisier

## 1. Introduction

Confined space natural convection flows are present in many natural phenomena and industrial processes; cooling electronic circuits and nuclear reactors, building and solar thermal systems are all examples of their manifestation. Generally, in industry, these flows have a turbulent character that could have positive effects by improving heat and mass mixtures and transfers. Several numerical and experimental studies have focused on convection in rectangular cavities, regarding their geometric simplicity and their presence in several industrial applications. Performed studies do not concern only laminar regime, but extend to turbulent regime, which is the most often encountered flow regime in nature. Several experimental works have been used to validate turbulence numerical models in cavities. For example, (Cheesewright *et al.*, 1986), reported by Davidson (1990), Tian et Karayiannis (2000), and Betts and Bokhari (2000). Ambient control generates strong energy growth in refreshing sector. Ventilation has a major influence on thermal comfort and thermal installations efficiency. Thus, a good ventilation system can provide an environment which thermal conditions are comfortable with lower energy consumption. Ventilation is still a physical phenomenon sometimes difficult to understand and aeration prediction still a complex subject. For airflow and air distribution accurate prediction in cavities, lot of problems need to be solved especially appropriate turbulence models (Peng, 1998; Chen et Jiang, 1992; Murakami *et al.* 1995). In most cases, flow in vented cavities occurs with natural or mixed convection and at low Reynolds numbers. Chen (1988) tested eight turbulence models to predict natural convection, forced convection, mixed convection and impacting jets in cavities. He concluded that none of these models produced satisfactory results and he noticed that one model may be appropriate in one case and inappropriate in another. Thus, for each flow type, experimental ventilation seems essential to ensure relevance of any model. We carry-out a numerical study of an industrial case of a simplified model already realized in order to validate the numerical tool used for our study and to make it possible to optimize the heat exchanges and to avoid in particular local overheating on surfaces beams. The study concerns the mixed convection phenomena generated by a heating element within a closed cavity resulting from problems related to aerothermal flows in ventilated caissons (soft belly) which shelter plane air conditioning equipment (Toulouse, 2004). To simplify the industrial case, a single air conditioning pack is considered inside a closed cavity, it is represented by a rectangle maintained at a constant temperature to obtain a temperature difference within the closed cavity. A diagonal jet is imposed at the right wall top to obtain a maximum heat exchange; air outlet is located at the left wall bottom. Our work consists to conduct a numerical study of mixed convection for this configuration in turbulent regime (at a fairly large Grashof number), in order to

treat this physical phenomenon aspects and analyze this industrial case conformity. For this, we divided our work into two parts. In the first part, we expose the configuration dealing with natural convection problem in a closed cavity, in order to validate our numerical tool, while the second part is dedicated to the numerical study of the mixed convection in turbulent regime in the ventilated cavities. We have mentioned the different numerical approaches, which differ by their degree of complexity and by additional equations that must be solved. The Launder and Sharma LRN k- $\epsilon$  model was used to close the equations system that governs the natural convection phenomenon in turbulent regime. In the study of mixed convection, the three turbulence models k- $\epsilon$  were used. The first study results are compared with the experimental ones given in. For mixed convection, a comparative study of turbulence models was conducted to adopt the most appropriate model for this cavity type and to study the ventilation effect on the cavity refreshment.

## 2. Mathematical formulation

### 2.1. Equations governing the flow

Averaged mass conservatory equation:

$$\frac{\partial}{\partial x_j} (\rho U_j) = 0 \quad (1)$$

Averaged movement quantity conservatory equation:

$$\frac{\partial}{\partial x_j} (\rho U_i U_j) = -\frac{\partial P}{\partial x_i} + \frac{\partial}{\partial x_j} (\tau_{ij} - \rho \overline{u_i u_j}) + S_M \quad (2)$$

Averaged energy conservatory equation:

$$\frac{\partial}{\partial x_j} (\rho U_j h_{tot}) = \frac{\partial}{\partial x_j} \left( \lambda \frac{\partial T}{\partial x_j} - \rho \overline{u_j h} \right) + \left[ U_i [\tau_{ij} - \rho \overline{u_i u_j}] \right] + S_E \quad (3)$$

Where  $\tau$  is the molecular constraint tensor.  $S_M$  is the source term added for floatability calculation:

$$S_{M,buoy} = (\rho - \rho_{ref}) \mathbf{g}$$

Total average enthalpy is given by:

$$h_{tot} = h + \frac{1}{2} U_i U_i + k$$

Total enthalpy contains a turbulent kinetic energy contribution,  $k$ , given by:  $k = \frac{1}{2} \overline{u_i^2}$ .

## 2.2. Turbulent viscosity models

The simplified approach represented by the turbulent viscosity hypothesis is that of the hypothesis formulated a century ago by Boussinesq, which consists of expressing algebraically the Reynolds tensor deviator algebraically as a function of the average strain rate:

$$-\rho \overline{u_i u_j} = \mu_t \left( \frac{\partial u_i}{\partial x_j} + \frac{\partial u_j}{\partial x_i} \right) - \frac{2}{3} \delta_{ij} \left( \rho k + \mu_t \frac{\partial u_k}{\partial x_k} \right) \quad (4)$$

Where  $\mu_t$  is the turbulent viscosity which links the turbulent kinetic energy to its dissipation via the relation:  $\mu_t = \rho C_\mu \frac{k^2}{\varepsilon}$ .

### 2.2.1. Standard model k-ε

This model is based on the turbulent dynamic viscosity concept, where the viscosity  $\mu_t$  is expressed as a function of the turbulent kinetic energy  $k$  and of its dissipation rate  $\varepsilon$ :  $\mu_t = \rho C_\mu \frac{k^2}{\varepsilon}$ .

The quantities  $k$  and  $\varepsilon$  are obtained by solving their respective transport equations which complete the system of equations (Launder et Spalding, 1972). In this model,  $C_\mu$  is a constant equal to 0.09.

### 2.2.2. RNG k-ε model

The RNG k-ε model, developed by Yakhot and Orszag (1986), is based on the so-called "renormalization" theory of the Navier-Stokes equations. The transport equations for turbulent generation and dissipation rate are the same as those for the standard k-ε model, but the constants for this model are analytically found using the RNG theory.  $C_\mu = 0.0845$ ,  $C_{\varepsilon 1} = 1.42$ ,  $C_{\varepsilon 2} = 1.68$ ,  $\sigma_T = 0.9$ ,  $\sigma_k = 1.0$ ,  $\sigma_\varepsilon = 1.3$ .

### 2.2.3. «Realizable» k-ε model

The "realizable" model was developed by Shih *et al.* (1995). The name of the model, "realizable" comes from the fact that the model provides some mathematical constraints on the Reynolds tensor.  $C_\mu$  in this model is no longer constant but its expression is formulated considering the average deformations of fluid and turbulence.

### 2.2.4. k-ε model at low Reynolds number

Low Reynolds Number (LRN models) turbulence models are models designed for low velocity flows. With these models, modifications have been made to the k-ε model to consider the turbulence progressive attenuation in the wall vicinity. Depreciation functions were introduced directly into these models and into the expression's turbulent viscosity and turbulent Prandtl number. Flow near the solid walls is therefore solved without adding any law or explicit function. The first LRN

k-ε model was developed by Jones and Launder (1973) and modified by several other researchers. Among the most popular "LRN" models are: Launder and Sharma (1974), Lam and Bremhorst (1981), Yang and Shih (1993), Abid (1993), Abe *et al.* (1994), Chang *et al.* (1995). These models differ from each other in the formulation of extra-terms damping functions and the condition at ε limit at the wall.

### 2.2.5. Low Reynolds k-ε model of Launder-Sharma (Bredberg, 2001)

For k-ε models,  $\mu_t = C_\mu \rho f_\mu \frac{k^2}{\varepsilon}$  and  $C_1 = 2.55$ ,  $C_{\varepsilon 1} = 1.44$ ,  $C_{\varepsilon 2} = 1.92$ ,  $C_\mu = 0.09$ ,  $\sigma_k = 1.0$  and  $\sigma_\varepsilon = 1.3$  are empiric constants, while  $f_1$ ,  $f_2$  and  $f_\mu$  are damping functions, typically used for « LRN » (k-ε) models. They allow these models to be available in the near-wall region.

$$v_t = C_\mu f_\mu \frac{k^2}{\varepsilon} \quad (5)$$

$$f_\mu = \exp \left[ \frac{-3.4}{\left(1 + \frac{Re_\varepsilon}{50}\right)^2} \right] \quad (6)$$

$$\frac{Dk}{Dt} = P_k - \varepsilon - 2\nu \left( \frac{\partial \sqrt{k}}{\partial x_j} \right)^2 + \frac{\partial}{\partial x_j} \left[ \left( \nu + \frac{v_t}{\sigma_k} \right) \frac{\partial k}{\partial x_j} \right] \quad (7)$$

$$P_k \approx v_t \left( \frac{\partial U_i}{\partial x_j} + \frac{\partial U_j}{\partial x_i} \right) \frac{\partial U_i}{\partial x_j} \quad (8)$$

$$\frac{D\varepsilon}{Dt} = C_{\varepsilon 1} \frac{\varepsilon}{k} P_k - C_{\varepsilon 2} f_2 \frac{\varepsilon^2}{k} + 2\nu v_t \left( \frac{\partial^2 U_i}{\partial x_j^2} \right) + \frac{\partial}{\partial x_j} \left[ \left( \nu + \frac{v_t}{\sigma_k} \right) \frac{\partial \varepsilon}{\partial x_j} \right] \quad (9)$$

$$f_2 = 1 - 0.3 \exp(-Re_\varepsilon^2) \quad (10)$$

## 3. Configurations and boundary conditions

Both configurations are similar in size and boundary conditions. The first represents the natural convection, schematized in figure .1 and the second represents the mixed convection schematized in figure .2. The geometry is a rectangular cavity 0.425 m high, 0.625 m long with a rectangle heating element of 0.216 x 0.140 m<sup>2</sup> placed as shown in the figure. The vertical walls are adiabatic and the lower and upper walls are maintained at a temperature  $T_w = 300$  K. A temperature distribution is imposed on the heating bar walls  $T_{e1}=350$ °K which leads to a number of Grashof based on the cavity containment height,  $Gr_H = 1,2.10^8$ . The ventilated cavity is equipped with a blow slot in the right wall upper part and a recovery in the left wall lower part, of respective heights equal to 0.006 m and 0.01 m. Air is blown inside the cavity at a temperature  $T_f=300$ °K and at a discharge velocity  $U_j$  from 9 m/s to 28 m/s, which corresponds to a Reynolds number built on the blow slot height  $Re_D$  between  $3,48.10^3$  et  $10^4$ . The inlet turbulence parameters are given by the following formulas:  $I = 0.16(Re_D)^{-1/8}$  et  $l = 0.07D$ , which gives a turbulence intensity between 5% and 6 % for our cases and the characteristic scale is  $4.2 \times 10^{-4}$ .

Discretized equations resolution is carried out by "Coupled" algorithm, diffusion terms are interpolated by a second order spatial scheme and convection terms are interpolated by the second order "Upwind" scheme. In both configurations, the mesh used is about 80200 cells refined near the walls. The low-Reynolds  $k-\epsilon$  model is applied in natural convection study of the closed cavity while  $k-\epsilon$  models (standard, realizable and RNG) are used in mixed convection study of the ventilated cavity.

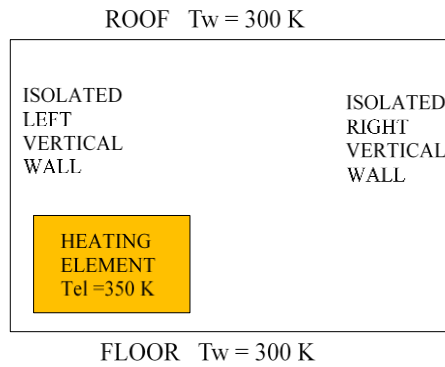


Figure 1. Configuration in natural convection

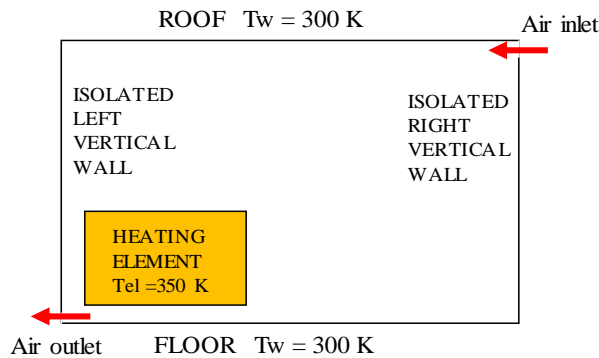


Figure 2. Configuration in mixed convection

## 4. Results and discussion

### 4.1. Configuration in natural convection

#### 4.1.1. Flow dynamic structure

The flow has a global single-cell structure; the resulting plume is deflected and

peeled off the walls for almost the same positions in the cavity. Quantitatively, velocities magnitude order is identical (about 0.25 m/s), figure 3. The air heats up on contact with the hot vertical walls maintained at 77°C of the element which leads to an increase in velocity over the upper corners of the hot source. The numerical simulation using the commercial code "Fluent" takes over the dynamic structure of the turbulent natural convection flow in the closed cavity with a heating bar.

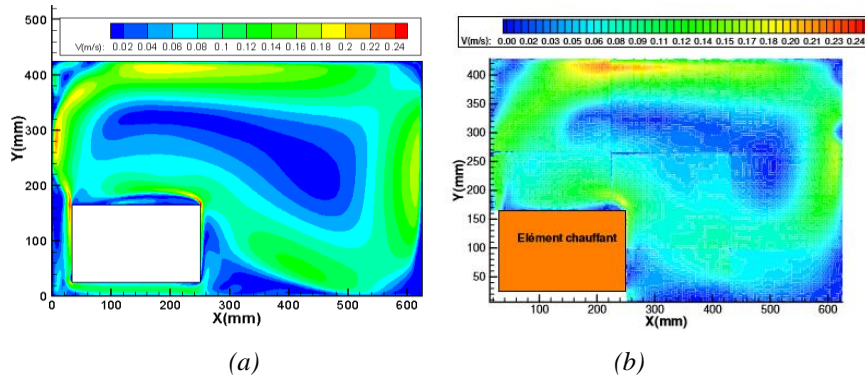


Figure 3. Dynamic field obtained by numerical simulation: (a) our numerical results (b) experimental results (Toulouse, 2004).

#### 4.1.2. Velocity profiles

Figures 4 and 5 show the average velocity profiles (numerical and experimental) according to the cavity height  $X = 200$  mm and  $Y = 200$  mm. From an overall point of view, both profiles look the same with an underestimation about 9% for the numerical calculation for  $X$  and about 10% for  $Y$  and this can be explained by the radiation negligence via numerical calculation.

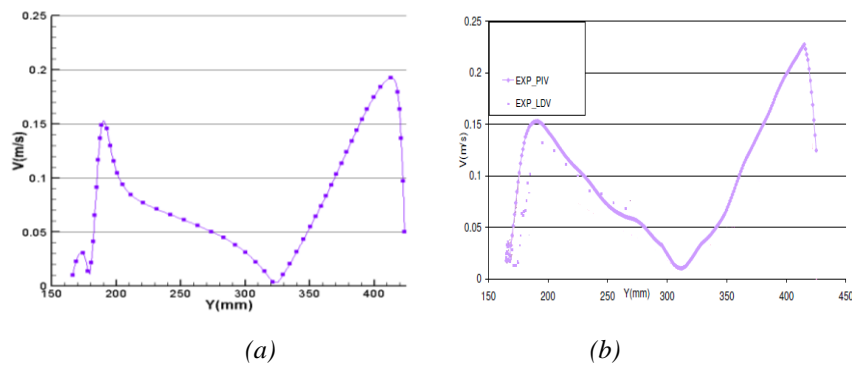


Figure 4. Average velocity profile at  $X=200$  mm (a) numerical (b) experimental

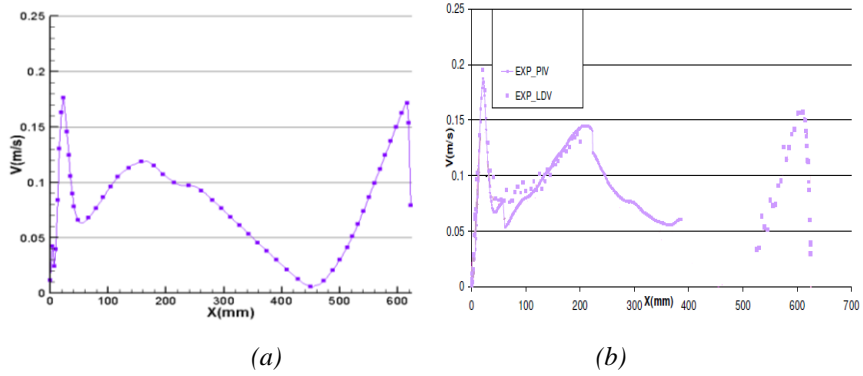


Figure 5. Average velocity profile at  $Y=200$  mm (a) numerical (b) experimental

#### 4.1.3. Thermal structure

Global temperature field in the cavity, obtained respectively, by numerical simulation and experiment is represented by figure 6. Note that the flow follows the cavity and hot source walls either for numerical or experimental.

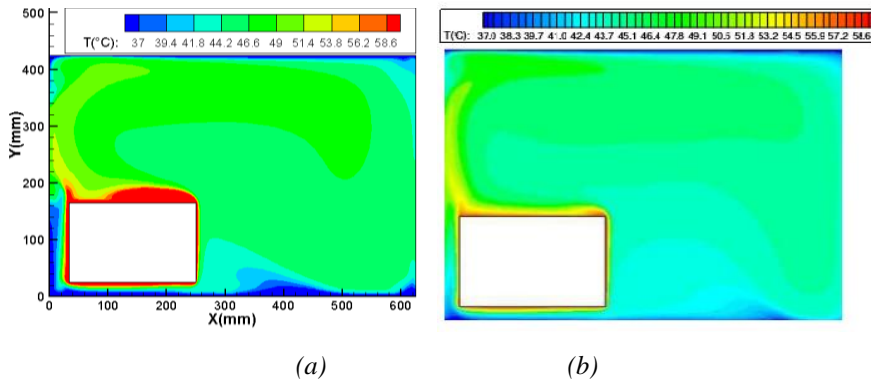


Figure 6. Thermal field (a) numerical (b) experimental

#### 4.1.4. Temperature profiles

Temperatures obtained via simulation are close to temperatures measured experimentally, an underestimation of the magnitude on the cavity left vertical wall by Fluent calculation code which can be explained by the fact that the numerical neglects the radiation created by the heating element (Figure 7). In conclusion, a great qualitative and quantitative correspondence of our numerical results with experimental ones.

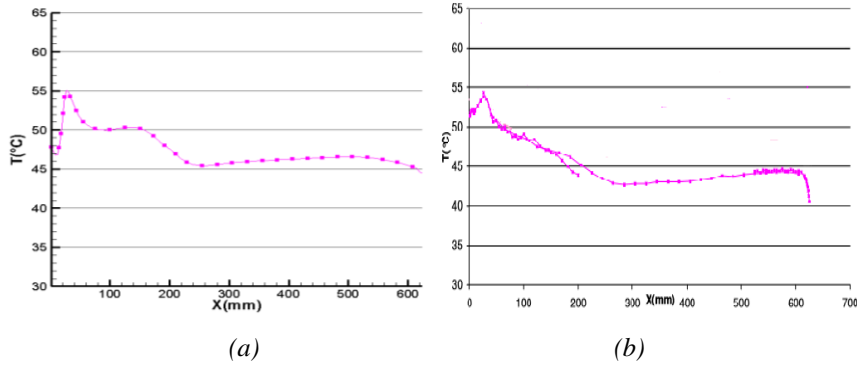


Figure 7. Temperature profile at Y=200 mm (a) numerical (b) experimental

4.1.5. Heat flow balance

Table 1 represents the heat flow balances in watts on the model walls and the hot source (numerical and experimental). The comparison of the results indicates a gap of not more than 7% for the loss in the upper wall and a difference of not more than 0.34% for the lower wall. The difference is especially noticeable on the left and right wall. This difference is caused by the adiabaticity which is not perfect in the experimental tests.

Table 1. Heat flow balance on each cavity wall

| Cavity      |              | Left | Right | Upper  | Lower  | Bar   |
|-------------|--------------|------|-------|--------|--------|-------|
| Balance [W] | Experimental | 5.8  | -3.1  | -51.2  | -26.1  | 74.6  |
|             | Numerical    | 0    | 0     | -47.40 | -25.93 | 74.37 |

4.1.6. Turbulent kinetic energy

Generally, turbulent kinetic energy is well reproduced by the calculation code "Fluent" (Figure 8). The turbulent kinetic energy is expressed in 2D by:  $K = \frac{u'^2 v'^2}{2} (m^2/s^2)$

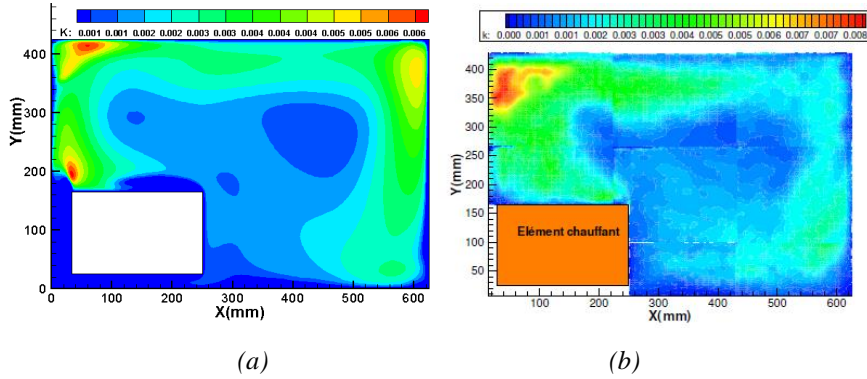


Figure 8. Turbulent kinetic energy (a) numerical (b) experimental

Table 2. Turbulent kinetic energy punctual measures (experimental & numerical)

|  |                  |     |     |          |          |          |          |          |          |          |
|--|------------------|-----|-----|----------|----------|----------|----------|----------|----------|----------|
| X (mm)   |                  | 250 | 200 | 150      | 100      | 80       | 80       | 100      | 150      | 200      |
| Y (mm)   |                  | 200 | 200 | 200      | 200      | 200      | 300      | 300      | 375      | 375      |
| K<br>(m <sup>2</sup> /s <sup>2</sup> )*10 <sup>3</sup> | Experimenta<br>l | 1.4 | 2.4 | 2.5      | 3.2      | 2.6      | 3.5      | 3.4      | 3.8      | 3.9      |
|  | Numerical        | 1.2 | 1.4 | 1.7<br>6 | 2.6<br>3 | 3.2<br>1 | 1.3<br>2 | 1.3<br>2 | 2.0<br>6 | 2.3<br>3 |

Table 2 represents punctual measurements of turbulent kinetic energy obtained by PIV compared to that simulated by Fluent (studied case) at these same measurement points. The numerical results are close to the experimental ones except that there is a slight underestimation of the values for the numerical result at the cavity center.

#### 4.1.7. Nusselt number

Nusselt number is defined by  $Nu = \frac{\varphi_{convected}}{\varphi_{conducted}}$ , where  $\varphi_{convected}$  is the heat flow density convected at the wall and  $\varphi_{conducted}$  is the heat flow density exchanged in pure conduction for a characteristic temperature difference in a flow layer of characteristic thickness (Djanna, 2011). Convected flow density can be expressed by  $\varphi_{cv} = -k\vec{\nabla}T \cdot \vec{n}$  and the conducted flow by  $\varphi_{cd} = \frac{k}{d}(T_b - T_0)$ . Local Nusselt number becomes:  $Nu = -\frac{\partial T^+}{\partial n}_{wall}$ . On the figure, we note that Nusselt number is high on bar surface corners, especially at right side corners [c, d], this is due to the strong curvature of streamlines locally at these two corners levels. Flow in these locations benefits from high velocity, consequently the heat transfer is large.

The noticed fluid detachment on the bar upper wall causes a layer which prevents the heat transfer from the solid to the fluid; therefore, we have a weak Nusselt on this part. In average value, Nusselt number on the bar right side is the highest, figure 9.

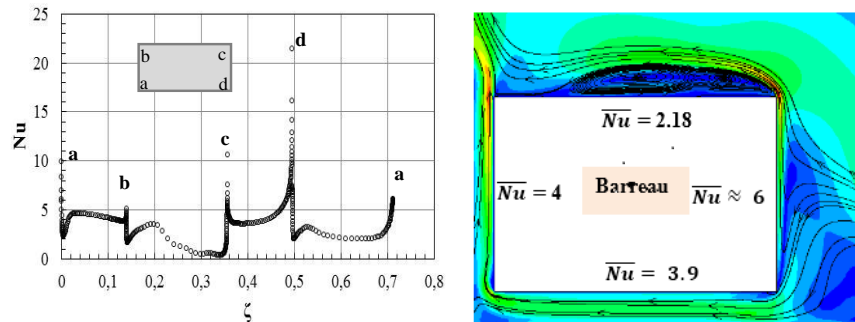
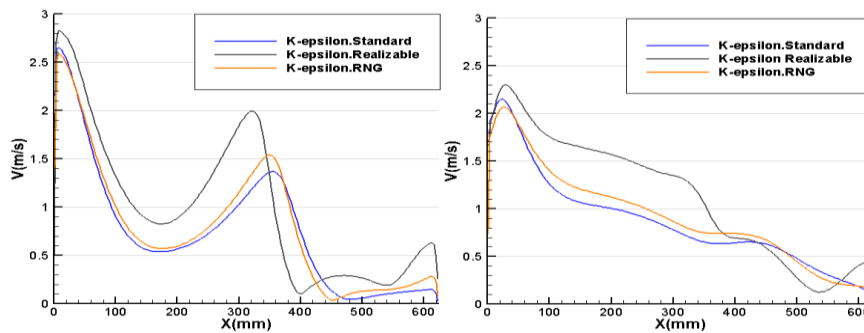


Figure 9. Local Nusselt number around the bar (Turbulent natural convection  $\Delta T=50^{\circ}C$ )

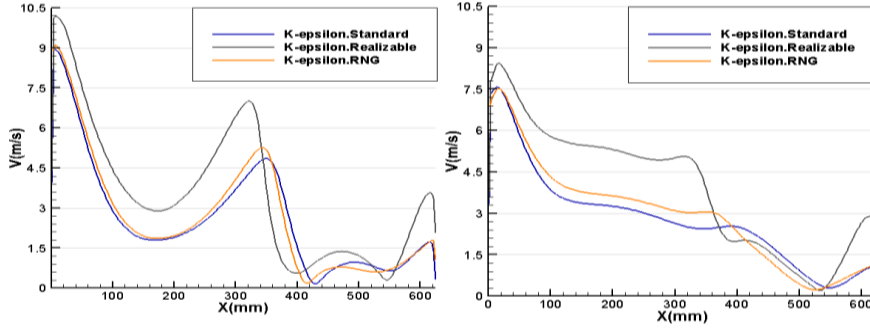
#### 4.2. Configuration in mixed convection

##### 4.2.1. Turbulence model validation

Due to the lack of experimental results in this study and in order to reach a choice of turbulence model suitable for our problem (mixed turbulent flow), a comparison was made between the three turbulence models k-ε which are proposed by the calculation code "Fluent": k-ε Standard, k-ε Realizable and k-ε -RNG. Velocity and temperature profiles visualization for two positions ( $Y/H_0 = 0.6$  and  $0.8$ ) is considered as comparison point between these turbulence models. Velocity and temperatures profiles representation for Richardson different numbers ( $Ri = 10$  and  $1$ ) are shown in Figures 10 and 11.

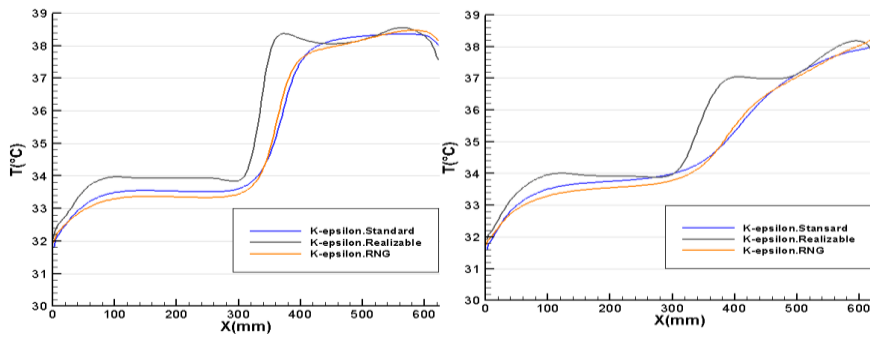


$Ri=10$  ( $V=9m/s$ )

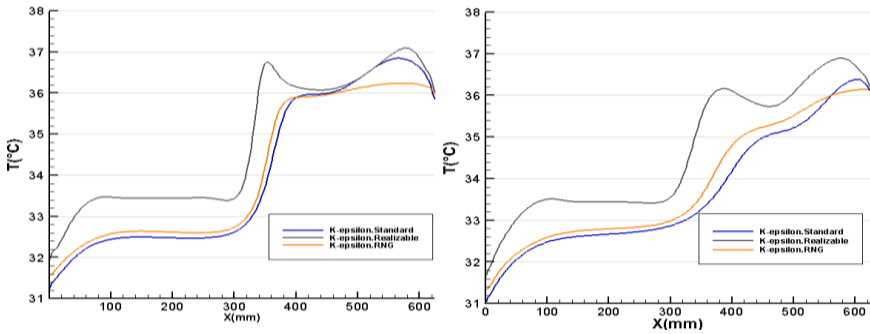


$Ri=1$  ( $V=28m/s$ )

Figure 10. Velocity profile viewing for different turbulence models and for each  $Ri$  (left:  $Y/H0=0.6$  & right:  $Y/H0=0.8$ )



$Ri=10$  ( $V=9m/s$ )



$Ri=1$  ( $V=28m/s$ )

Figure 11. Temperature profiles viewing for different turbulence models & for each  $Ri$  (left:  $Y/H0=0.6$  & right:  $Y/H0=0.8$ )

For the two types of turbulent convection, the three turbulence models give similar profiles for either velocity or temperature, it is clear that the curves have the same trend. The  $k-\epsilon$  Realizable model overestimates remarkably the flow properties values (velocity and temperatures) compared to the other standard  $k-\epsilon$  and RNG  $k-\epsilon$  models, which allows us to override it for this choice, the other two models ( $k-\epsilon$  standard and  $k-\epsilon$  RNG) have very close values. Note that for velocity, maximum difference is about 12% when  $Ri$  decreases. Same for temperature values, difference between the two models is about 3%. These two models are the most used for turbulent flows studies away from walls and for quite important velocities. For our case, we will choose the model  $k-\epsilon$  RNG because it is the suitable model for flows in ventilated cavities as well as flows with recirculation (Wang, 2009).

4.2.2. Flow dynamic structure

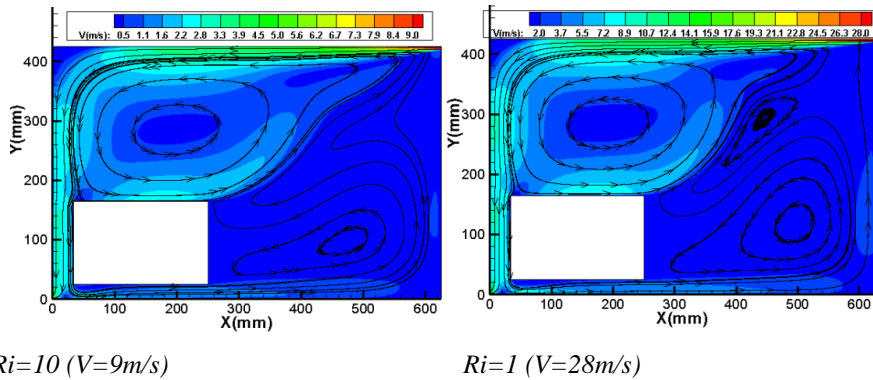


Figure 12. Dynamic fields in ventilated cavity for Richardson different numbers (RNG  $k-\epsilon$  model)

To start the dynamic study, we visualize the average velocity field in the studied cavity by drawing the streamlines on the contours using the software "Tecplot" for the two  $Ri$  numbers (10 and 1) in Figure12. The dynamic field shows us that the flow comprises two parts in the cavity. The first part represents flow localized above the heating element which forms a recirculation area with fairly high velocities and the second part represents the area outside the heating element and which forms a low recirculation area at low velocities. The flow is bicellular for input velocity  $U_{j1}=9\text{m/s}$ , the appearance of a third cell is visualized in the streamlines when the input velocity increases ( $U_{j2}=28\text{m/s}$ ). The incoming air jet is seen by the plume formed along the cavity upper wall and then downward due to contact with the left adiabatic wall. Part of the observed plume continues to go down into the channel formed between the heating element and the cavity left wall to reach the cavity air outlet opening. The plume second part sticks and runs along the heating element upper wall. We notice that the plume detachment from this wall is diverted towards the cavity upper right corner (towards the jet inlet) and then redo the circuit, which shows us the influence of the vertical velocities formed by the air heating near the element right vertical wall

(natural convection) on the large horizontal velocities, which dominate the flow on the bar upper wall that are caused by the jet velocities at the origin (forced convection). The flow down the area between the element and the cavity left wall is divided into two parts, one exiting through the discharge opening, and the other part along the cavity lower wall and then up the right vertical wall which explains the appearance of the plume in these areas where it becomes more apparent by increasing the inlet velocity.

#### 4.2.3. Thermal fields

Thermal fields obtained for jet different input velocities are visualized in Figure 13. Jet introduction causes a distribution of heat inside the cavity, the hot air due to the hot source is driven towards the cavity right part, temperature decreasing in this part is observed when the jet inlet velocities increase, and the coldest area is the one above the heating element, so globally the coldest flow is the best ventilated flow.

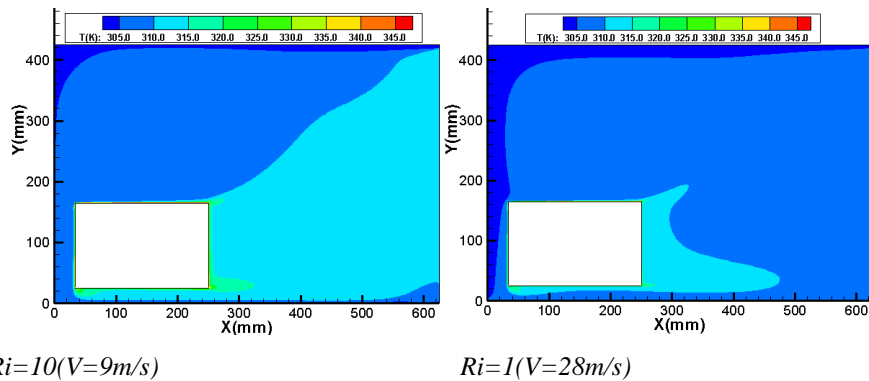


Figure 13. Thermal fields of different jet inlet velocities into the cavity

#### 4.2.4. Nusselt number

The cooling process is of vital and essential interest; therefore, the main purpose of this study is the cooling of the bar and the refreshing of the cavity. In order to have a high heat transfer from the bar to the fluid and consequently a maximum local Nusselt, the air jet was introduced at ambient temperature and at different velocities. From Figure 14, we note that the local Nusselt numbers along the different faces of the bar have similar profiles regardless the jet velocity value. We also note that the Nusselt number on the bar faces increases considerably when  $U_j$  increases ( $Ri$  decreases). This increase is mainly observed on the upper face [bc] and right [cd] of the bar. This is mainly due to the disappearance of the recirculation area which leads to a significant increase in the local Nusselt number in this region. Quantitatively, the jet velocity increase from 9 m/s to 28 m/s improves the average Nusselt number about 50%, 60%, 60% and 70% [da] faces, respectively, figure 15.

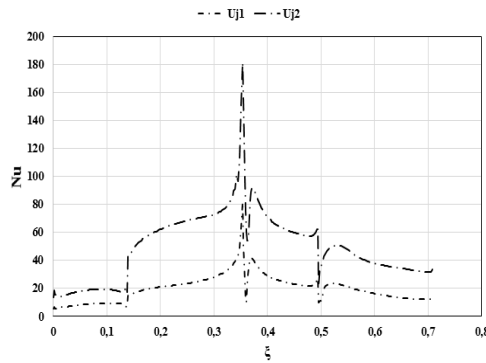


Figure 14. Local Nusselt number around the bar

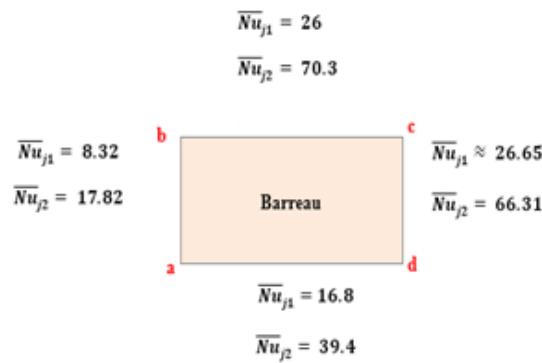


Figure 15. Average Nusselt for each bar face (Turbulent mixed convection, different  $Ri$ )

### 5. Conclusion

The study we conducted allowed prevention of physical phenomena acting in closed and ventilated cavities. The mixed turbulent convection flow has been approved based on a study of the turbulence model choice. First, we conducted a comparative study between three turbulence models (standard  $k-\epsilon$ ,  $k-\epsilon$  RNG and  $k-\epsilon$  Realizable) in order to choose the most appropriate model for our case. Based on the literature and our study, the  $k-\epsilon$  RNG model is found to be best suited to turbulent flows with recirculation in ventilated cavities. The results are found satisfactory for the cooling of the heating bar heating source and the refreshing of the cavity by comparing the flows in natural and mixed convection.

## References

- Abe K., Kondoh T., Nagano Y. (1994). A new turbulence model for predicting fluid flow and heat transfer in separating and reattaching flows - I. Flow field calculations. *Int. J. Heat Mass Tran.*, Vol. 37, pp. 139-151. [https://doi.org/10.1016/0017-9310\(94\)00252-Q](https://doi.org/10.1016/0017-9310(94)00252-Q)
- Abid R. (1993). Evaluation of two-equation turbulence models for predicting transitional flows. *Int. J. Eng. Sci.*, Vol. 31, pp. 831-840. [https://doi.org/10.1016/0020-7225\(93\)90096-d](https://doi.org/10.1016/0020-7225(93)90096-d)
- Betts P. L., Bokhari I. H. (2000). Experiments on turbulent natural convection in an enclosed tall cavity. *International Journal of Heat and Fluid Flow*, Vol. 21, pp. 675-683. [https://doi.org/10.1016/S0142-727X\(00\)00033-3](https://doi.org/10.1016/S0142-727X(00)00033-3)
- Bredberg J. (2001). On two-equation eddy-viscosity models. Department of thermos fluid dynamics. *Internal report n°01/8*, 2001. *Chalmers university of technology*, Göteborg, Sweden.
- Chang K. C., Hsieh W. D., Chen C. S. (1995). A modified low-reynolds-number turbulence model applicable to recirculation flow in pipe expansion. *J. Fluids Eng.*, Vol. 117, No. 3, pp. 417-423. <https://doi.org/10.1115/1.2817278>
- Cheesewright R., King J. R., Ziai S. (1986). Experimental data for the validation of computer codes for the prediction of two-dimensional buoyant cavity flow. *ASME Winter Annual Meeting, Hemisphere HTD*, Vol. 60, pp. 75-81.
- Chen Q. (1988). Indoor airflow, air quality and energy consumption of buildings. Ph. D Thesis, *Delft University of Technology*, Netherlands.
- Chen Q., Jiang Z. (1992). Significant question in predicting room air motion. *ASHRAE Transactions*, Vol. 98, pp. 929-939.
- Davidson L. (1990). Second-order corrections of the k- $\epsilon$  model to account for non-isotropic effects due to buoyancy. *International Journal of Heat Mass Transfer*, Vol. 33, No. 12, pp. 2599-2608. [https://doi.org/10.1016/0017-9310\(90\)90195-Z](https://doi.org/10.1016/0017-9310(90)90195-Z)
- Djanna F. (2011). Convection naturelle turbulente a grands nombres de Rayleigh: Caractérisation expérimentale des écoulements et des transferts thermiques, étude numérique du couplage convection-rayonnement. *Thèse de Doctorat. Institut Pprime, ENSMA Poitiers*.
- Jones W. P., Launder B. E. (1973). The calculation of low-Reynolds number phenomena with a two-equation model of turbulence. *Int. J. Heat Mass Tran.*, Vol. 16, pp. 1119-1130. [https://doi.org/10.1016/0017-9310\(73\)90125-7](https://doi.org/10.1016/0017-9310(73)90125-7)
- Lam C. K., Bremhorst G. K. (1981). A modified form of the k- $\epsilon$  model for predicting wall turbulence. *Journal of Fluids Engineering*, Vol. 103, pp. 456-460.
- Launder B. E., Spalding D. B. (1972). *Lectures in Mathematical Models of Turbulence*, Academic Press, London. <https://doi.org/10.1234/12345678>
- Launder B. E., Sharma B. I. (1974). Application of the energy-dissipation model of turbulence to the calculation of flow near a spinning disc. *Letters in Heat and Mass Transfer*, Vol. 1, pp. 131-138. [https://doi.org/10.1016/0735-1933\(74\)90024-4](https://doi.org/10.1016/0735-1933(74)90024-4)
- Murakami S., Kato S., Kobayashi H., Henyu F. (1995). Current status of CFD application to air-conditioning engineering. *Pan Pacific Symposium on building and Urban Environmental Conditioning in Asia March 1995*, Nagoya, Japan.

- Peng S. H. (1998). Modelling of turbulent flow and heat transfer for building ventilation. Ph. D Thesis, *Chalmers University of Technology*, Sweden.
- Shih T. H., Liou W. W., Shabbir A., Yang Z., Zhu J. (1995). A New k- $\epsilon$  eddy viscosity model for high Reynolds number turbulent flows. *Computers and Fluids*, Vol. 24, No. 3, pp. 227-238. [https://doi.org/10.1016/0045-7930\(94\)00032-T](https://doi.org/10.1016/0045-7930(94)00032-T)
- Tian Y. S., Karayiannis T. G. (2000). Low turbulence natural convection in an air filled square cavity. Part I: The thermal and fluid flow fields. *International Journal of Heat and Mass Transfer*, Vol. 43, pp. 849-866.
- Toulouse M. L. (2004). Analyse et caractérisation de la convection naturelle et de la convection mixte dans des enceintes confinées. Thèse de Doctorat. *Ecole nationale supérieure de l'aéronautique et de l'espace*, ONERA, Centre de Toulouse.
- Wang X. (2009). Prédiction et analyse numérique d'écoulements turbulents avec transfert thermique dans des cavités ventilées à l'aide d'un modèle à relaxation elliptique. *Thèse de Doctorat*. Université de Lille 1.
- Yakhot V., Orszag S. A. (1986). Renormalization group analysis of turbulence I. *Basic theory J. Sci. Comput*, Vol. 11, pp. 1-51.
- Yang Z., Shih T. H. (1993). new time scale based k - $\epsilon$  model for near-wall turbulence. *American Institute of Aeronautics and Astronautics Journal*, Vol. 31, pp. 1191-1198. <http://arc.aiaa.org/doi/abs/10.2514/3.11752>

